THE JOURNAL OF PHYSICAL CHEMISTRY B

Article

pubs.acs.org/JPCB

Pressure-Induced Frustration–Frustration Process in 1-Butyl-3-methylimidazolium Hexafluorophosphate, a Room-Temperature Ionic Liquid

Hiroshi Abe,*[,†] Takahiro Takekiyo,[‡] Naohiro Hatano,[‡] Machiko Shigemi,[‡] Nozomu Hamaya,[§] and Yukihiro Yoshimura[‡]

[†]Department of Materials Science and Engineering and [‡]Department of Applied Chemistry, National Defense Academy, Yokosuka 239-8686, Japan

[§]Graduate School of Humanities and Sciences, Ochanomizu University, 2-1-1 Otsuka, Bunkyo-ku, Tokyo 112-8610, Japan

ABSTRACT: We have found that the room-temperature ionic liquid (RTIL) reveals outstanding pressure-induced phase changes from a liquid state to a crystal polymorph and finally to a glass form upon compression by up to 8 GPa. The RTIL is 1-butyl-3-methylimidazolium hexafluorophosphate, $[C_4mim][PF_6]$, which offers the opportunity to investigate a variety of fluctuations in one system and can be completely recovered without dissociation or polymerization, even after decompression. Similar to charge frustration, spin ice-like frustration, and geometric frustration in high potential spintronics/multiferroic materials, the RTIL frustrations are classified into charge (scalar), orientation (vector), and coordination number (topology). Degrees of freedom at each state of $[C_4mim][PF_6]$ are described by charge balancing, molecular orientational order/disorder, molecular conformations of the C_4mim^+ cation, and the coordination number. Here, we show a novel "conformation glass" induced by high pressure.

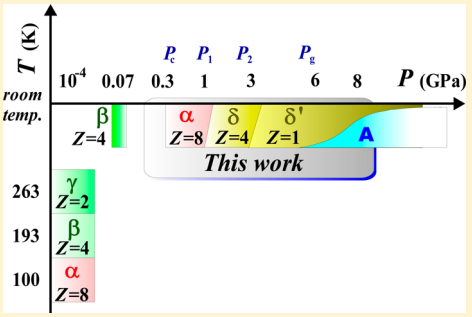

1. INTRODUCTION

Room-temperature ionic liquids (RTILs) are promising functional molten salts that are characterized by dominant Coulombic forces and are designed using a combination of an asymmetric large organic cation and an organic/inorganic anion. Being considered as recyclable "green solvents", the intrinsic properties of RTILs have been widely applied in various fields, including catalysts,[1] electrochemical devices,[2] and CO_2 separation techniques.[3] Among the different RTILs, 1-butyl-3-methylimidazolium hexafluorophosphate, $[C_4mim][PF_6]$ is an important ionic liquid, characterized by high CO_2 solubility under high pressure.[3] Moreover, CO_2 absorption/desorption by $[C_4mim][PF_6]$ is completely reversible even under high pressure. In the first generation of the RTILs, a series of 1-alkyl-3-methylimidazolium cations, $[C_nmim]$, with tetrafluoroborate, BF_4^-, and PF_6^- have been well-investigated as representative RTILs, where n represents the alkyl chain length.[4] Phase diagrams of $[C_nmim][BF_4]$ and $[C_nmim][PF_6]$ include the significant effect of the nonpolar alkyl chain length.

At ambient pressure, the arrangements of charge (scalar),[5] spin (vector),[6] and topological defects (coordination number)[7] on the lattice sites of the frustrated systems are significant factors that influence their material properties. Representative of a frozen charge system of an organic conductor, a charge glass as a new concept was included in the frustrated system. The disorder state obeys the conventional glass-forming theory on the two-dimensional (2D) triangular lattice.[5] It is well-known that the 2D triangular lattice involves the geometrical disorder component. Representative of a highly frustrated magnetic system, spin freezing resembling ice is realized on a 3D tetrahedral network (the pyrochlore lattice).[6] In addition to the 2D triangular system, the tetrahedron is regarded as a unit in the most frustrated 3D system. Geometrical disorder on the pyrochlore lattice is distinguished by spin. The residual configurational entropy of spin is evaluated by the simple ice rule. Representative of a geometric frustration in a ferroelectric system, nanosized patterns appear, relating to the defects on the compositionally modulated ferroelectrics.[7] Defect-driven instability causes topological textures. The idea of chirality derived from an electric dipole leads to the complicated patterns.

Our goal is to investigate the intrinsic frustration–frustration process in one system only. In this study, we focus on $[C_4mim][PF_6]$ as a prototype of a RTIL. The $[C_4mim][PF_6]$ system offers the advantage to investigate a variety of frustrations because it has charge, molecular orientational order, molecular conformations,[8−10] and crystal polymorphs both at low temperatures[11−16] and under pressures below 4 GPa.[17−22] Herein, we demonstrate successive frustrations of charge, orientation, and conformations on periodic/nonperiodic sites in $[C_4mim][PF_6]$ upon compression by up to 8 GPa at room temperature by using in situ X-ray diffraction and Raman spectroscopy. Consistent with the phase change, a pressure-induced partially

Received: October 7, 2013
Revised: December 19, 2013

   dx.doi.org/10.1021/jp409924h | J. Phys. Chem. B XXXX, XXX, XXX−XXX

constrained gauche conformation relating to the off-positioned PF_6^- anion was detected from the Raman spectra.

2. EXPERIMENTAL SECTION

$[C_4mim][PF_6]$ (Kanto Chemical Co.) was selected as the ionic liquid in this study. Water contamination in the sample was checked using the Karl Fischer method and was confirmed to be less than 100 ppm in the sample.

High-pressure X-ray diffraction experiments were carried out by using a Mao-Bell type diamond anvil cell (DAC) in the BL-18C of the Photon Factory at the High Energy Accelerator Research Organization in Japan.[23] Inside of the glovebox, the sample and ruby balls were loaded into the 0.35 mm hole of a preindented stainless gasket with a thickness of 0.180 mm in the DAC. A microbeam with a diameter of 100 μm was obtained using the collimator. For the high-pressure experiments, the maximum pressure used was 8.1 GPa. Two-dimensional (2D) diffraction patterns were obtained using an Imaging-Plate system (BAS2000, Fuji-Film Co., Japan). Subsequently, the 2D data were converted to one-dimensional intensity data in order to minimize the preferred orientation on the Debye rings. The pressure was also determined from the spectral shift of the R_1 fluorescence line of the ruby balls in the sample chamber of the DAC. The scattered angles, 2θ, and the incident wavelength, λ (=0.6199 Å), were calibrated by a standard CeO_2 polycrystalline. The observed powder diffraction patterns were analyzed by using the ab initio structure determination program *FOX* (free objects for crystallography).[24] Molecular arrangements were simulated by optimizing the molecule parametrization for global optimization algorithms.

High-pressure Raman spectra were measured using a Raman spectrophotometer (NR-1800, Jasco Co.) equipped with a single monochromator and a charge coupled device detector. A Lexel Ar^+ laser of wavelength 514.5 nm and power 250 mW was used as an excitation source. For performing the high-pressure experiment, the sample was put into a screw type DAC. The pressure was monitored from the R_1 fluorescence line of the ruby balls, which were packed inside of the DAC. The high pressure of 8.2 GPa was achieved by the combination of type-I diamonds (culet 0.8 mm) and a stainless steel gasket with a diameter of 0.25 mm and a thickness of 0.082 mm.

3. RESULTS AND DISCUSSION

3.1. Crystallization during Compression Observed by High-Pressure X-ray Diffraction. In-situ observation of high-pressure X-ray diffraction was performed at room temperature in order to find the new high-pressure phase of $[C_4mim][PF_6]$. Figure 1 exhibits the X-ray diffraction patterns under high pressure, where the scattering wave vector, Q, is represented as $4\pi\cdot(\sin\theta)/\lambda$ [Å^{-1}]. Liquid samples easily crystallize at 0.3 GPa (=P_c). The black and red solid curves in Figure 1 indicate the observed and calculated X-ray diffraction patterns, respectively. The calculated patterns are obtained by *FOX*.[24] Crystallographic data from the present and previous studies[22] are summarized in Table 1. As can be seen from the data, the crystal structures of the high-pressure and low-temperature α phases are equivalent. Further compression led to the discovery of a monoclinic crystal structure above 1 GPa (=P_1), coexisting with the α phase. This monoclinic phase had no relation with the low-temperature crystals such as orthorhombic α and triclinic β and γ phases.[22] Herein, we denote this phase as the δ phase to distinguish it from the α, β, and γ crystals (Figure 2).

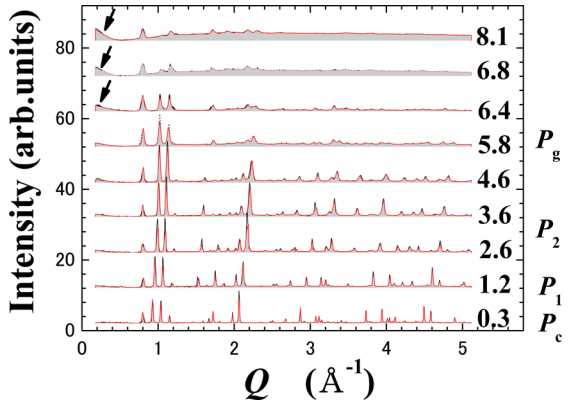

Figure 1. High-pressure X-ray diffraction patterns during the compressing process. The pressure unit is GPa. P_c is the crystallization pressure. P_1 and P_2 stand for the first and second solid−solid phase transition pressures, respectively. P_g is the amorphous appearance pressure. Above 6 GPa, the low q component, which is indicated by the arrows, increased.

The space group of the δ phase is found to be monoclinic $P2/m$ (Z = 4), where Z stands for the number of molecules per unit cell.

Subsequently, structure analysis at around 3 GPa (=P_2) suggests that the second solid−solid phase transition occurred with the coexistence of two phases. Intriguingly, the high-pressure crystals of the monoclinic $P2/m$ (Z = 1) appeared at P_2 (Figure 2); the phases of these crystals are henceforth referred to as the δ' phase. To the best of our knowledge, the "Z = 1" lattice of the high-pressure crystal was discovered first in imidazolium-based RTILs. Therefore, it remains unclear as to why the δ' phase exhibits the Z = 1 lattice. Despite the coexistence of two phases, there still exist sharp Bragg peaks at 3.6 GPa (Figure 1). This implies negligible little lattice distortions or external hydrostatic pressure applied to the crystal.

Under high pressure, competitive interactions might be effective in the crystal state of the imidazolium-based cation. One such interaction is the repulsive $\pi-\pi$ interaction, as seen in aromatic materials, while the other is the dipole−dipole interaction in ionic crystals, such as alkali cyanides. In the case of the former, the geometrical constraint in a zigzag stacking sequence, based on the $\pi-\pi$ interactions such as benzene (Z = 4),[25] naphthalene (Z = 2),[26] and anthracene (Z = 2),[26] should be satisfied by a large unit cell ($Z \geq 2$). On the other hand, the latter behavior is well-known to occur in typical nonsymmetric molecules such as alkali cyanides. Alkali cyanides exhibit polymorphism ($Z \geq 2$) upon varying the orientational order of CN ions by application of pressure. At ambient pressure, cyanides exhibit pseudocubic lattice structure (Z = 4) owing to free rotation of the CN ions.[27,28] As one exception, the tetragonal phase IV ($P4mm$, Z = 1) in NaCN appeared above a pressure of 15 GPa, where perfect ordering of CN develops along the c direction.[27] In contrast to alkali cyanides that exhibit only one molecular conformation, the conformational variety of the C_4mim^+ cation can be used to explain the Z = 1 lattice of the phase as follows: its orientational disorder at the lattice sites satisfies the $P2/m$ symmetry.

3.2. Amorphization upon Compression Observed by High-Pressure X-ray Diffraction. Upon further compression, we noticed a significant feature at 5.8 GPa (=P_g), which was quite different from the solid−solid phase transitions at P_1 and P_2. This feature signifies the "pressure-driven amorphization

dx.doi.org/10.1021/jp409924h | J. Phys. Chem. B XXXX, XXX, XXX−XXX

Table 1. Crystallographic Data Obtained from the Previous and Present Studies[22a]

T (K)	P (GPa)	space group	a (Å)	b (Å)	c (Å)	β (deg)	Z	ρ (g/cm^3)	wR	R
				Previous Work						
298	ambient liq.							1.373		
193	ambient	*Pbca*	9.4924	9.8406	26.8817	90 99.219(α)	8	1.503	0.155	0.048
293	0.07	$P\bar{1}$	9.5818	9.5826	14.5801	99.252(β) 99.667(γ)	4	1.477	0.2113	0.074
				Present Work						
293	0.3	*Pbca*	9.365	9.731	27.031	90	8	1.532	0.308	0.288
293	1.2	*Pbca*	9.416	9.706	26.806	90	8	1.541	0.294	0.364
293	1.2	*P*2/*m*	11.965	7.802	13.109	109.7	4	1.638	0.208	0.217
293	2.6	*P*2/*m*	11.997	7.837	13.057	109.6	4	1.632	0.260	0.317
293	3.6	*P*2/*m*	12.005	7.822	13.016	109.5	4	1.639	0.128	0.141
293	3.6	*P*2/*m*	6.004	7.822	6.579	109.0	1	1.615	0.175	0.192
293	4.6	*P*2/*m*	5.967	7.822	6.575	109.6	1	1.632	0.196	0.167
293	5.8	*P*2/*m*	5.821	7.970	6.494	106.9	1	1.637	0.152	0.182
293	6.4	*P*2/*m*	5.683	7.976	6.388	105.1	1	1.688	0.132	0.156
293	6.8	*P*2/*m*	5.573	7.961	6.297	103.0	1	1.733	0.0629	0.060
293	8.1									

[a]The weighted reliability and conventional factors are expressed as wR and R, respectively.

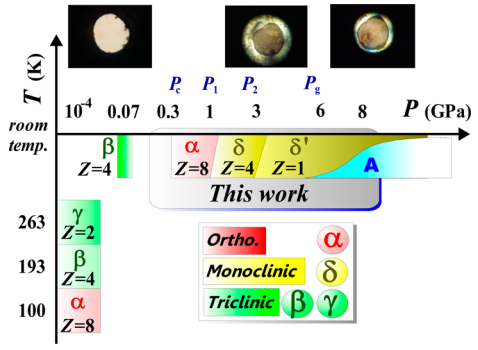

Figure 2. Schematic pressure−temperature diagram relating to the crystals combined with the previous studies. A stands for amorphous. The direct optical microscope images are provided as insets in the figure. The left optical microscope image in the liquid is transparent. The partial transparent right picture reveals partial amorphization above P_g.

from crystal" without polymerization[25,29−33] or dissociation,[34−40] wherein typical topological frustration is induced with breaking the periodic array of ions. Generally, pressure-induced amorphization in molecular systems occurs accompanying the molecular damages. Polymerization under high pressures is generally irreversible after decompression, once the pressure-induced polymeric phases appear. In contrast to the polymerization, molecular dissociations are driven by high pressure, accompanied by an insulator to metallic transition. Focusing on amorphization in ionic systems, the pressure-induced irreversible C═N polymerization of NaCN appears at around 38 GPa.[27] The unexpected amorphization observed in the present study can be explained based on the following experimental facts: (i) the broad diffraction halo gradually increases above 5.8 GPa, (ii) peak broadening and a decrease in the intensity of Bragg reflections can be observed, (iii) the low Q component, which is indicated by the arrows in Figure 1, increases above 5.8 GPa, and (iv) the sample is transformed to a partial transparent state, as observed by using optical microscopy (insets of Figure 2). On the basis of the results (i)−(iii), it can be assumed that amorphization and grain refining of the crystal occurs simultaneously. According to fundamental diffraction theory,[41] the halo pattern would have originated from molecular orientational/positional disorder, and fine particles contribute to both small-angle X-ray scattering and peak broadening of the Bragg reflections in X-ray diffraction patterns. The result (iv) implies the state change of the sample at the macroscopic level (optical microscopic image shown as an inset in Figure 2). Before compression, the transparent sample in the liquid and ruby balls can be monitored clearly. Here, it is highly advantageous to determine the crystallization from liquid. Direct visual determination by using optical microscopic images can distinguish not only the liquid−solid phase transition but also the solid−solid phase transitions. The movements of the crystal domains could be easily observed using the optical microscope. After crystallization, the crystal domain boundaries in the optical image become darker. Above P_g, the gradual appearance of the amorphous phase inside of the crystal is indicated by the partial brightness in the sample. This optical transparency of the amorphous phase is based on the concept of a homogeneous and nonboundary state of the amorphous phase. Therefore, results (i)−(iv) substantiate the high-pressure-induced amorphization in the crystal, both microscopically and macroscopically.

In general, pressurized ionic crystals tend to be energetically stabilized on the periodic lattice due to a shorter molecular distance under high pressure. Despite the simplicity of the molecular system, the periodic array of the cation and anion is broken under high pressure. This can be resolved by considering that it is the Z = 1 monoclinic lattice just below the glass transition pressure. The Z = 1 lattice is characterized by the orientational disorder of the cation, with disappearance of the positional/orientational modulations of the δ phase (Z = 4). As a precursor phenomenon of the amorphization, a $\pi-\pi$ stacking sequence between the imidazolium rings is completely lost.

3.3. Molecular Conformations upon Compression. It is of significant importance to understand whether $[C_4mim][PF_6]$ is retrieved or not after the decompression. Molecular damages can be easily examined by using Raman spectra. Raman spectra of liquid states before/after compression are measured in the high and low wavenumber regions (Figure 3a and b), where

dx.doi.org/10.1021/jp409924h | J. Phys. Chem. B XXXX, XXX, XXX−XXX

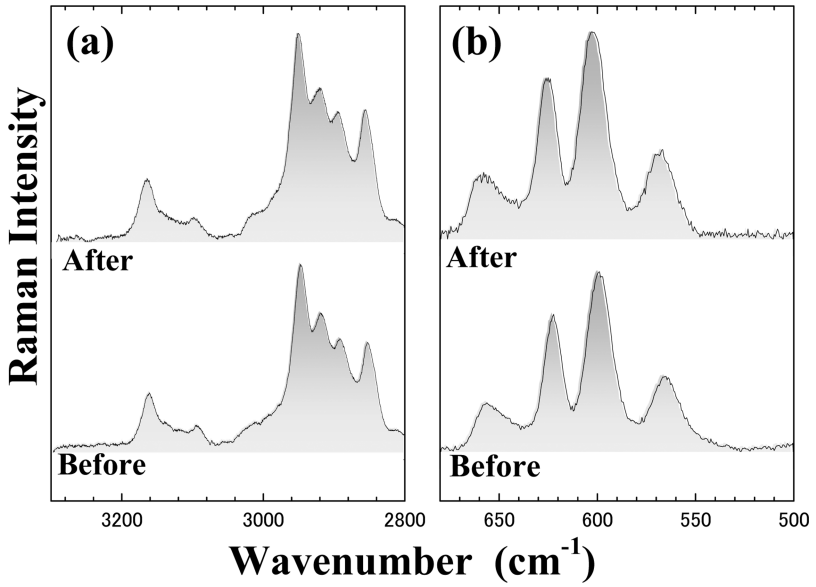

Figure 3. Raman spectra before/after compression at the (a) CH stretching region and (b) low wavenumber region. After compression up to 8.2 GPa, the sample completely recovered without polymerization or dissociation.

the maximum pressure, P_{max}, is 8.2 GPa. The similarity of the spectra before/after compression proves that the $[C_4mim][PF_6]$ is completely recovered without molecular damage under high pressure.

In addition to the molecular arrangements determined by X-ray diffraction, molecular conformation is a key to explore hidden conformational frustration in a molecular system. A direct correlation between the conformational equilibrium and phase transition is so far well-documented.[8,9] In the C_4mim^+ cation, α, β, and γ crystals of $[C_4mim][PF_6]$ at low temperature and ambient pressure are characterized by a portion of the gauche−trans (GT), trans−trans (TT), and gauche′−trans (G′T) for the butyl chain, respectively (Figure 4a−c).[14−16] At first, we mention the liquid state of $[C_4mim][PF_6]$ as seen in the bottom spectrum in Figure 5a. In the liquid, it is also established that the ∼625 and ∼600 cm^{-1} peaks in the CH_2 rocking mode are assigned to be trans (T) and gauche (G) conformers relating to NCCC rotation, respectively.[42,43] In the spectrum in Figure 5a, red and black peaks, which are obtained by the curve fitting analysis method, reveal trans and gauche conformers. Furthermore, the 560 cm^{-1} peak is assigned to the PF_6^- vibrational mode, which is denoted by an open circle in the figure.

Our next step is to investigate the conformation changes against pressure from Raman CH_2 rocking spectra. At 0.6 GPa (=P_c), crystallization occurs accompanied by domain wall movement, as observed in the optical microscope. Concordant with the peak changes, the trans conformer in the Raman spectrum decreases drastically at P_c. In the first solid−solid phase transition at around 1 GPa (=P_1), a broad peak of the PF_6^- vibrational mode separates into two peaks, which are marked by two open circles. The peak splitting has a connection with the δ phase (Z = 4), where the lattice is explained by two different sites of the PF_6^-.

Above 3 GPa (=P_2), the Raman spectra intriguingly exhibited a new peak at 605 cm^{-1} (3.5 GPa), as drawn by the blue peak in the Figure 5a. This was observed for the first time in this study. This new peak with lower wavenumber may be attributed to the gauche conformer rather than trans one, such as the partially

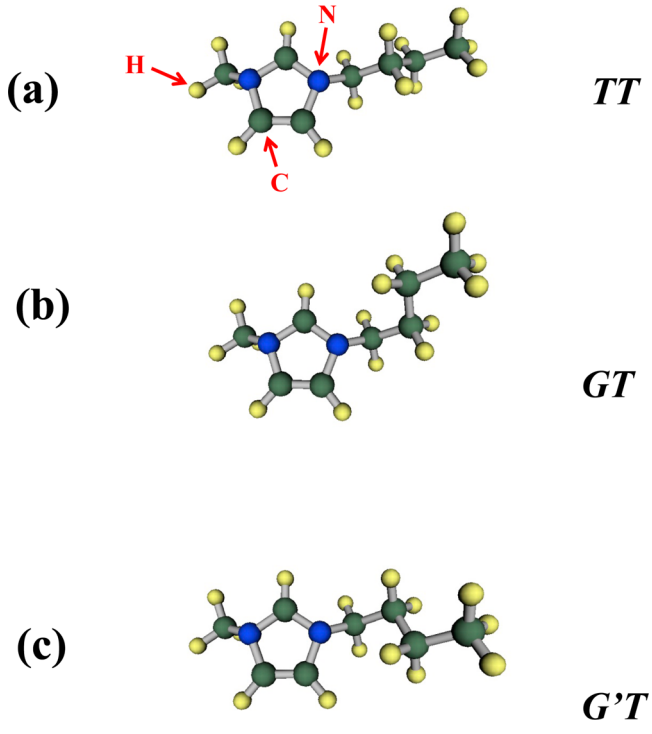

Figure 4. C_4mim^+ conformations of (a) TT, (b) GT, and (c) G′T.

constrained gauche at high pressure. We support that the new peak might be related to the gauche conformer, such as the spatially constrained gauche conformer at high pressure. Here, we tentatively name the new peak as G_c. In section 3.4, we will explain in more detail about the new peak. At the same time, the trans conformer almost disappears within experimental error. Instead of the trans conformer (having a straight alkyl chain), the new pressure-induced peak (G_c) mainly occupies above P_2. Therefore, at P_2, the crossover from T to G_c which corresponds to a crystal polymorph from δ (Z = 4) to δ' (Z = 1), occurs as determined by X-ray diffraction. This suggests that G_c can be regarded as one of the factors of the Z = 1 lattice.

dx.doi.org/10.1021/jp409924h | J. Phys. Chem. B XXXX, XXX, XXX−XXX

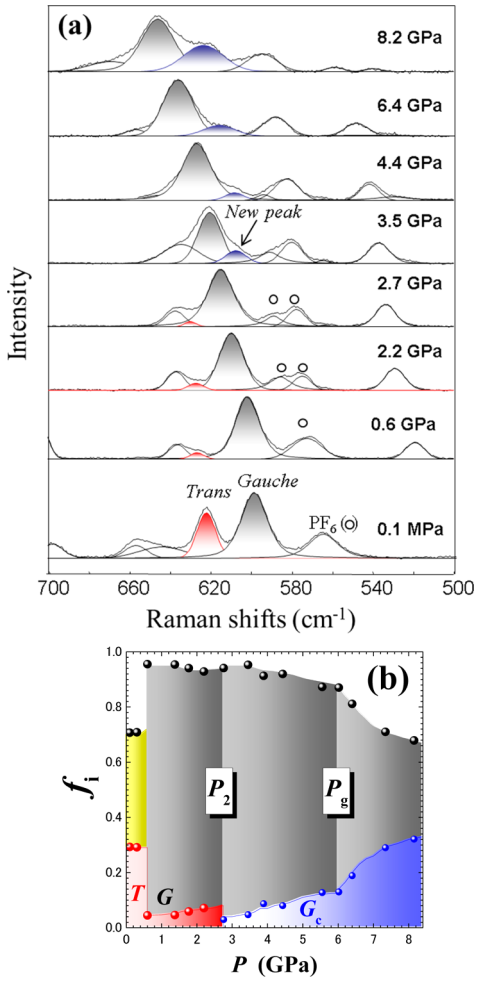

Figure 5. Raman spectra under high pressure. (a) Pressure dependence of CH_2 rocking modes of the C_4mim^+ cation and (b) intensity fraction, f_i, of T, G and G_c conformers. Open circles reveal the PF_6^- vibrational mode. Closed blue circles reveal the pressure-induced G_c conformer. Red and black peaks correspond to T and G modified by highly packed circumstances.

Above 6 GPa (=P_g), two significant experimental facts were obtained clearly. One is that the peak intensity of the new peak increased drastically. The other is that peak splitting of the PF_6^- vibrational mode completely disappeared. Considering the observed Raman spectra on the compression process, distinct changes appeared at P_c, P_1, P_2, and P_g, whose pressures correspond to phase changes determined by X-ray diffraction. For a further understanding of the results, a variety of conformations should be analyzed quantitatively. Focusing on the C_4mim^+ conformer, we calculated the intensity fraction of the i component, f_i (Figure 5b), where i stands for the trans (T), gauche (G), and spatially constrained gauche (G_c) conformers. Here, f_i (i = T, G, and G_c) is introduced as[21]

$$f_i = \frac{I_i}{I_T + I_G + I_{Gc}} \quad (1)$$

where I_T, I_G, and I_{Gc} indicate the relative Raman intensity of the trans (T), gauche (G), and spatially constrained gauche (G_c) conformers, respectively. In the quantitative plot (Figure 5b), P_c, P_2, and P_g are clearly provided by discrete changes of f_i. On the other hand, P_1 in the Raman spectra is characterized by the peak splitting of the PF_6^- vibrational mode. A comparison of the X-ray diffraction patterns and Raman spectra suggests that the hidden frustrations are extracted exactly by molecular conformations and crystal structures, depending on the molecular distance under high pressure. Similar to the optical observation results during X-ray diffraction, the optical observation during Raman analysis indicates the appearance of the partially transparent part in the sample above P_g.

3.4. Simulation Correlating the X-ray Diffraction Patterns. Recent computer-aided analysis using X-ray diffraction patterns can evaluate molecular conformations on the lattice sites. In the simulation box, the possible conformers of C_4mim^+ cations are determined by ab initio calculation. In order to resolve the amorphization inside of the $Z = 1$ lattice, Monte Carlo simulations were carried out using *FOX*.[24] Molecular decorations and conformations on the lattice sites are optimized referring to the observed diffraction patterns ($\sin(\theta)/\lambda < 0.25$ Å^{-1}). In the simulations, a simple antibump constraint is employed as a penalty between a cation and an anion to prevent molecular overlapping. Also, hydrogen of the C_4mim^+ cation is taken into account in the constraint not to overlap with an anion, although hydrogen is not sensitive in X-ray diffraction. Under the above-mentioned conditions, no two molecules are closer than the minimum distance. In addition, conformations of cation and anion are flexible in the simulations, while the fixed occupation probabilities, p_i (i = G and G_c), are set at each pressure.

In order to clarify the amorphous contribution to the $Z = 1$ lattice, simulations are carried out using the observed data at 4.6 ($P < P_g$), 5.8 ($P \approx P_g$), and 6.4 GPa ($P_g < P$). At 4.6 GPa ($P < P_g$) without an amorphous phase, we prepare the gauche conformer ($p_G = 0.92$) and spatially constrain the gauche conformer ($p_{Gc} = 0.08$), where p_i is obtained by the intensity fraction, f_i, in Raman spectroscopy (Figure 5b). After 10^7 iterations, relative positions between the cation and anion at 4.6 GPa are optimized (Figure 6a). Hydrogen is not visualized to emphasize the butyl chain. In the gauche conformer, the butyl chain is folded, as predicted theoretically.[10] In the actual lattice, molecules having the gauche and spatially constrained gauche conformers are superimposed by each occupation probability in the unit cell, satisfying the $P2/m$ symmetry. Here, we noticed that two different kinds of intermolecular distances between cation and anion (Table 2) express the molecular packing efficiency and a collapse of the charge network under high pressure. Thus, we define that the distance, r_i (i = G and G_c), corresponds to a length between the center of the imidazolium ring and the phosphorus. The calculated r_i are summarized in Table 2. At the same time, the average distance, r_{ave}, is given as $p_G r_G + p_{G_c} r_{G_c}$. Below P_g, each r_i (i = G, G_c, and ave), is comparable.

At 5.8 GPa ($P \approx P_g$), the occupation probabilities are p_G = 0.87 and p_{G_c} = 0.13. The further folding gauche conformer is also favorable with shorter distance (r_G) in the simulation box (Figure 6b). Despite lattice shrinking under high pressure, r_{G_c} becomes larger. The anion is shifted away from the imidazolium ring of the spatially constrained gauche conformer. This means that under high pressure, the charge network between the cation and anion is partially broken at G_c.

Proportional to the progress of amorphization, the above tendencies are enhanced at 6.4 GPa ($P_g < P$), as shown in Figure 6c. In the simulations at 6.4 GPa, the fixed p_G = 0.81 and p_{G_c} = 0.19 are used. A picture of much shorter r_G and a further folding gauche conformer enables it to introduce the

dx.doi.org/10.1021/jp409924h | J. Phys. Chem. B XXXX, XXX, XXX−XXX

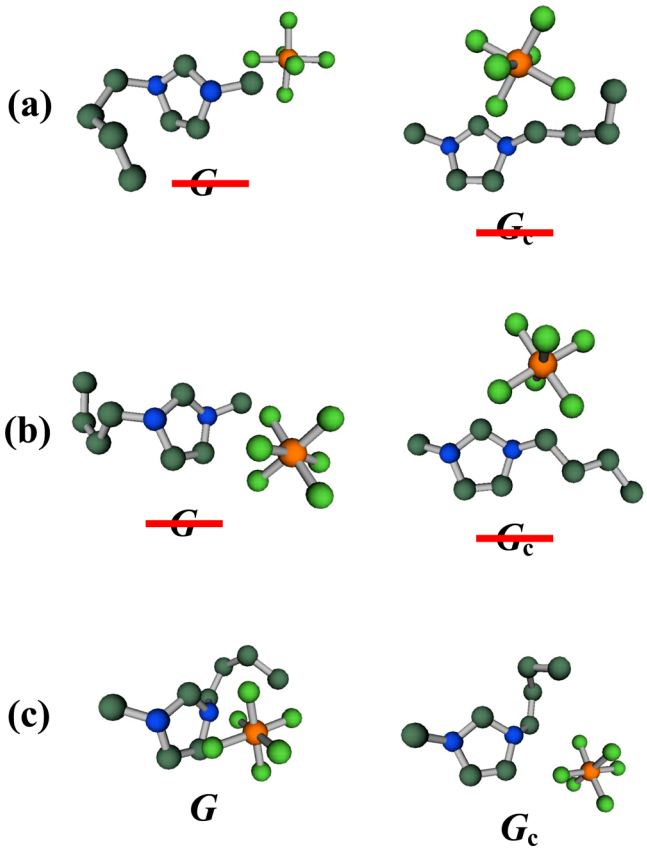

Figure 6. Simulated molecular conformations correlating the X-ray diffraction patterns. (a) G and G_c conformers at 4.6 GPa ($P < P_g$), (b) G_r and G_c conformers at 5.8 GPa ($P \approx P_g$), and (c) G and G_c conformers at 6.4 GPa ($P_g < P$). To emphasize folding of the butyl chain, hydrogen is not displayed, although hydrogen is used in the simulations to not overlap with the anion.

Table 2. Intermolecular Distance between the Cation and Anion Calculated by Global Optimization[a]

P (GPa)	p_G	p_{Gc}	r_G (Å)	r_{Gc} (Å)	r_{ave} (Å)
4.6	0.92	0.08	4.755	4.533	4.738
5.8	0.87	0.13	3.956	4.807	4.067
6.4	0.81	0.19	2.777	4.869	3.174

[a]The distance, r_i (i = G, G_c, and ave), is measured from the central phosphorus to the center of the imidazolium ring. By Raman spectra, p_i (i = G and G_c) is obtained from the intensity fraction, f_i, in Figure 5b.

"ion pairing" of the cation and anion. It seems that the anion is captured between the alkyl chain and the imidazolium ring of the cation. The nearly spherical ion pairing disturbs the stacking sequence of the imidazolium ring. Electrostatically, positive and negative charge is compensated for locally in the ion pairing. Geometrically, the spherical pairing causes the orientational disorder on the lattice site. Therefore, nonionic crystal-like characteristic might be realized. On the other hand, the off-positioning of the anion is promoted considering the relatively larger r_{G_c} at 6.4 GPa. Therefore, we deduce that charge compensation (shorter r_G) and charge network breaking (longer r_{G_c}) occur simultaneously above P_g.

3.5. Competitive Disorder Factors Induced by High Pressure. Over the whole pressure region, high-pressure-induced crystallization and amorphization in $[C_4mim][PF_6]$ are comprehended based on the conformational variety of the

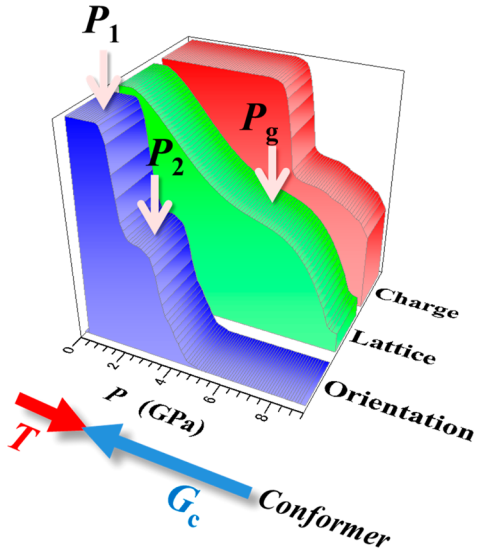

Figure 7. Schematic illustration of molecular conformations and frustrations on the pressure scale. T is a conformer that is derived from a liquid disorder, while G_c, which has the off-positioned PF_6^- anion from the imidazolium ring, might be regarded as solid disorder on a high-pressure amorphous conformer. The two different kinds of disorder factors depend on the loosely or densely packed circumstances.

C_4mim^+ cation. The representative trans (liquid-like) and spatially constrained gauche (amorphous-like) conformers are proposed as competitive disorder factors on the pressure scale (Figure 7). A series of the frustrations is expressed by a combination of charge, orientation, and lattice based on the T and G_c. To gain further insight into the effect of conformation, the experimental results are interpreted based on the orientational glass in mixed systems of alkali cyanides at ambient pressure and low temperature.[44−46] In $(KCN)_x(NaCN)_{1-x}$ having unique conformation, the glass is induced by freezing of the randomly oriented CN ions. However, the glass in the mixed system is suppressed under high pressure. Only by the orientational frustration, high-pressure glass cannot be realized due to well-arrayed molecules for dense packing.

Above P_g, different competition occurred due to the highly dense packing. According to the ab initio simulation referring to X-ray diffraction, the ion pairing (orientational disorder) and the "off-positioned anion" (positional disorder) disturb the long-range well-balanced charge network. Furthermore, inhomogeneous coexistence of gauche conformer (charge compensation with shorter r_G) and constrained gauche conformer (charge network breaking with longer r_c) enables it to develop the disorder.

Recent results of the *N*,*N*-diethyl-*N*-methyl-*N*-(2-methoxyethyl) ammonium tetrafluoroborate ($[DEME][BF_4]$) system also support the connection of cation folding and "antiparallel pairing" of the cation with phase instabilities of both low-temperature and high-pressure crystals.[47] We prove that, in the metastable crystals, the positive and negative charge network was interrupted at the cation pairing.

4. CONCLUDING REMARKS

We have succeeded to demonstrate the novel pressure-induced frustration−frustration process in one system only with a case of $[C_4mim][PF_6]$. Under high pressure, a variety of C_4mim^+ conformations causes the successive frustrations, charge (scalar), orientation (vector), and coordination number

dx.doi.org/10.1021/jp409924h | J. Phys. Chem. B XXXX, XXX, XXX−XXX

(topology). On the basis of the results, we introduce "conformation glass" of the C_4mim^+ cation as a new concept. The potential impact of the findings presented in this study has an implication on the free-energy landscape[48] at a nonequilibrium state and fills in gaps to the relation between degrees of freedom of motions and entropic stabilization in condensed matter physics.

AUTHOR INFORMATION

Notes

The authors declare no competing financial interest.

ACKNOWLEDGMENTS

This work was supported by Photon Factory Research Project (Proposal #: 2010G546).

REFERENCES

(1) Leitner, W. A Greener Solution. *Nature* **2003**, *423*, 930−931.
(2) Armand, M.; Endres, F.; MacFarlane, D. R.; Ohno, H.; Scrosati, B. Ionic-Liquid Materials for the Electrochemical Challenges of the Future. *Nat. Mater.* **2009**, *8*, 621−629.
(3) Blanchard, L. A.; Hancu, D.; Beckman, E. J.; Brennecke, J. F. Green Processing Using Ionic Liquids and CO_2. *Nature* **1999**, *399*, 28−29.
(4) Holbrey, J. D.; Seddon, K. R. Ionic Liquids. *Clean Products Proc.* **1999**, *1*, 223−236.
(5) Kagawa, F.; Sato, T.; Miyagawa, K.; Kanoda, K.; Tokura, Y.; Kobayashi, K.; Kumai, R.; Murakami, Y. Charge-Cluster Glass in an Organic Conductor. *Nat. Phys.* **2013**, *9*, 419−422.
(6) Kimura, K.; Nakatsuji, S.; Wen, J.-J.; Broholm, C.; Stone, M. B.; Nishibori, E.; Sawa, H. Quantum Fluctuations in Spin-Ice-Like $Pr_2Zr_2O_7$. *Nat. Commun.* **2013**, *4*, 1934.
(7) Choudhury, N.; Walizer, L.; Lisenkov, S.; Bellaiche, L. Geometric Frustration in Compositionally Modulated Ferroelectrics. *Nature* **2011**, *470*, 513−517.
(8) Talaty, E. R.; Raja, S.; Storhaug, V. J.; Dölle, A.; Carper, W. R. Raman and Infrared Spectra and Ab Initio Calculations of C_{2-4}mim Imidazolium Hexafluorophosphate Ionic Liquids. *J. Phys. Chem. B* **2004**, *108*, 13177−13184.
(9) Tsuzuki, S.; Arai, A. A.; Nishikawa, K. Conformational Analysis of 1-Butyl-3-methylimidazolium by CCSD(T) Level Ab Initio Calculations: Effects of Neighboring Anions. *J. Phys. Chem B* **2008**, *112*, 7739−7747.
(10) Zhao, Y.; et al. The Behavior of Ionic Liquids under High Pressure: A Molecular Dynamics Simulation. *J. Phys. Chem. B* **2012**, *116*, 10876−10884.
(11) Dibrov, S. M.; Kochi, J. K. Crystallographic View of Fluidic Structures for Room-Temperature Ionic Liquids: 1-Butyl-3-methylimidazolium Hexafluorophosphate. *Acta Crystallogr., Sect. C* **2006**, *62*, o19−21.
(12) Choudhury, A. R.; Winterton, N.; Steiner, A.; Cooper, A. I.; Johnson, K. A. *In Situ* Crystallization of Low-Melting Ionic Liquids. *J. Am. Chem. Soc.* **2005**, *127*, 16792−16793.
(13) Triolo, A.; et al. Thermodynamics, Structure, And Dynamics in Room Temperature Ionic Liquids: The Case of 1-Butyl-3-methyl Imidazolium Hexafluorophosphate ([bmim][PF_6]). *J. Phys. Chem. B* **2006**, *110*, 21357−21364.
(14) Endo, T.; Kato, T.; Tozaki, K.; Nishikawa, K. Phase Behaviors of Room Temperature Ionic Liquid Linked with Cation Conformational Changes: 1-Butyl-3-methylimidazolium Hexafluorophosphate. *J. Phys. Chem. B* **2010**, *114*, 407−411.
(15) Endo, T.; Murata, H.; Imanari, M.; Mizushima, N.; Seki, H.; Nishikawa, K. NMR Study of Cation Dynamics in Three Crystalline States of 1-Butyl-3-methylimidazolium Hexafluorophosphate Exhibiting Crystal Polymorphism. *J. Phys. Chem. B* **2012**, *116*, 3780−3788.
(16) Endo, T.; Murata, H.; Imanari, M.; Mizushima, N.; Seki, H.; Sen, S.; Nishikawa, K. Comparative Study of the Rotational Dynamics of PF_6^- Anions in the Crystals and Liquid States of 1-Butyl-3-methylimidazolium Hexafluorophosphate: Results from ^{31}P NMR Spectroscopy. *J. Phys. Chem. B* **2013**, *117*, 326−332.
(17) Su, L.; Li, L.; Hu, Y.; Yuan, C.; Shao, C.; Hong, S. Phase Transition of [C_n-mim][PF_6] under High Pressure up to 1.0 GPa. *J. Chem. Phys.* **2009**, *130*, 184503/1−184503/4.
(18) Su, L.; Li, M.; Zhu, X.; Wang, Z.; Chen, Z.; Li, F.; Zhou, Q.; Hong, S. In Situ Crystallization of Low-Melting Ionic Liquid [BMIM][PF_6] under High Pressure up to 2 GPa. *J. Phys. Chem. B* **2010**, *114*, 5061−5065.
(19) Takekiyo, T.; Hatano, N.; Imai, Y.; Abe, H.; Yoshimura, Y. Pressure-Induced Phase Transition of 1-Butyl-3-methylimidazolium Hexafluorophosphate [bmim][PF_6]. *High Pressure Res.* **2011**, *31*, 35−38.
(20) Russina, O.; Fazio, B.; Schmidtc, C.; Triolo, A. Structural Organization and Phase Behaviour of 1-Butyl-3-methylimidazolium Hexafluorophosphate: An High Pressure Raman Spectroscopy Study. *Phys. Chem. Chem. Phys.* **2011**, *13*, 12067−12074.
(21) Shigemi, M.; Takekiyo, T.; Abe, H.; Yoshimura, Y. Pressure-Induced Crystallization of 1-Butyl-3-methylimidazolium Hexafluorophosphate. *High Pressure Res.* **2013**, *33*, 229−233.
(22) Saoaune, S.; Norman, S.; Hardacre, C.; Fabbiani, F. P. A. Pinning down the Solid-State Polymorphism of the Ionic Liquid [bmim][PF_6]. *Chem. Sci.* **2013**, *4*, 1270−1280.
(23) Shimomura, O.; Takemura, K.; Fujihisa, H.; Fujii, Y.; Ohishi, Y.; Kikegawa, T.; Amemiya, Y.; Matsushita, T. Application of an Imaging Plate to High-Pressure X-ray study with a Diamond Anvil Cell. *Rev. Sci. Instrum.* **1992**, *63*, 967−973.
(24) Favre-Nicolin, V.; Cerny, R. FOX, 'Free Objects for Crystallography': A Modular Approach to *Ab Initio* Structure Determination from Powder Diffraction. *J. Appl. Crystallogr.* **2002**, *35*, 734−743.
(25) Wen, X.-D.; Hoffmann, R.; Ashcroft, N. W. Benzene under High Pressure: A Story of Molecular Crystals Transforming to Saturated Networks, With a Possible Intermediate Metallic Phase. *J. Am. Chem. Soc.* **2011**, *133*, 9023−9035.
(26) Williams, D. E.; Xiao, Y. Benzene, Naphthalene and Anthracene Dimers and Their Relation to the Observed Crystal Structures. *Acta Crystallogr., Sect. A* **1993**, *49*, 1−10.
(27) Chen, J.-Y.; Yoo, C.-S. Physical and Chemical Transformations of Sodium Cyanide at High Pressures. *J. Chem. Phys.* **2009**, *131*, 144507/1−144507/7.
(28) Strössner, K.; Hochheimer, H. D.; Hönle, W.; Werner, A. High-Pressure Raman and X-ray Studies of the Alkali Cyanides up to 27 GPa. *J. Chem. Phys.* **1985**, *83*, 2435−2440.
(29) Ciabini, L.; Santoro, M.; Gorelli, F. A.; Bini, R.; Schettino, V.; Raugei, S. Triggering Dynamics of the High-Pressure Benzene Amorphization. *Nat. Mater.* **2007**, *6*, 39−43.
(30) Citroni, M.; Bini, R.; Foggi, P.; Schettino, V. Role of Excited Electronic States in the High-Pressure Amorphization of Benzene. *Proc. Natl. Acad. Sci. U.S.A.* **2008**, *105*, 7658−7663.
(31) Santoro, M.; Gorelli, F. A.; Bini, R.; Ruocco, G.; Scandolo, S.; Crichton, W. A. Amorphous Silica-Like Carbon Dioxide. *Nature* **2006**, *441*, 857−860.
(32) Iota, V.; Yoo, C.-S.; Klepeis, J.-H.; Jenei, Z.; Evans, W.; Cynn, H. Six-Fold Coordinated Carbon Dioxide VI. *Nat. Mater.* **2007**, *6*, 34−38.
(33) Sun, J.; Klug, D. D.; Martoňák, R.; Montoya, J. A.; Lee, M.-S.; Scandolo, S.; Tosatti, E. High-Pressure Polymeric Phases of Carbon Dioxide. *Proc. Natl. Acad. Sci. U.S.A.* **2009**, *106*, 6077−6081.
(34) Hemley, R. J. Effects of High Pressure on Molecules. *Annu. Rev. Phys. Chem.* **2000**, *51*, 763−800.
(35) Gregoryanz, E.; Goncharov, A. F.; Hemley, R. J.; Mao, H. High-Pressure Amorphous Nitrogen. *Phys. Rev. B* **2001**, *64*, 052103/1−052103/14.
(36) Dean, D. W.; Wentzcovitch, R. M.; Keskar, N.; Chelikowsky, J. R. Pressure-Induced Amorphization in Crystalline Silica: Soft Phonon Modes and Shear Instabilities in Coesite. *Phys. Rev. B* **2000**, *61*, 3303−3309.

(37) Wezka, K.; Salmon, P. S.; Zeidler, A.; Whittaker, D. A. J.; Drewitt, J. W. E.; Klotz, S.; Fischer, H. E.; Marrocchelli, D. Mechanisms of Network Collapse in GeO_2 Glass: High-Pressure Neutron Diffraction with Isotope Substitution As Arbitrator of Competing Models. *J. Phys.: Condens. Matter* **2012**, *24*, 502101/1−502101/9.
(38) Kruger, M. B.; Meade, C. High-Pressure Structural Study of GeI_4. *Phys. Rev. B* **1997**, *55*, 1−3.
(39) Ohmura, A.; Sato, K.; Hamaya, N.; Isshiki, M.; Ohishi, Y. Structure of Pressure-Induced Amorphous Form of SnI_4 at High Pressure. *Phys. Rev. B* **2009**, *80*, 054201/1−054201/7.
(40) Grocholski, B.; Speziale, S.; Jeanloz, R. Equation of State, Phase Stability, And Amorphization of SnI_4 at High Pressure and Temperature. *Phys. Rev. B* **2010**, *81*, 094101/1−094101/7.
(41) Warren, B. E. *X-ray Diffraction*; Dover: New York, 1990.
(42) Hamaguchi, H.; Ozawa, R. Structure of Ionic Liquids and Ionic Liquid Compounds: Are Ionic Liquids Genuine Liquids in the Conventional Sense? *Adv. Chem. Phys.* **2005**, *131*, 85−104.
(43) Umebayashi, Y.; et al. Dependence of the Conformational Isomerism in 1-*n*-Butyl-3-methylimidazolium Ionic Liquids on the Nature of the Halide Anion. *J. Phys. Chem. B* **2010**, *114*, 11715−11724.
(44) Mertz, B.; Berret, J. F.; Bohmer, R.; Meissner, M.; Knaak, W. Calorimetric Investigations of $(NaCN)_{1-x}(KCN)_x$ Glasses. *Phys. Rev. B* **1990**, *42*, 7596−7603.
(45) Cheng, A.; Klein, M. L.; Lewis, L. J. Competing Interactions and Orientational Ordering in $(NaCN)_{1-x}(KCN)_x$ Quadrupolar Glasses. *Phys. Rev. Lett.* **1991**, *66*, 624−627.
(46) Adolphi, N. L.; Conradi, M. S. Two-Part Freezing in the Orientational Glass $(KCN)_x(NaCN)_{1-x}$. *Phys. Rev. B* **1992**, *45*, 13057−13060.
(47) Abe, H.; Imai, Y.; Takekiyo, T.; Yoshimura, Y.; Hamaya, N. Low Temperature and High Pressure Crystals of Room Temperature Ionic Liquid: *N*,*N*-Diethyl-*N*-methyl-*N*-(2-methoxyethyl) Ammonium Tetrafluoroborate. *J. Phys.: Conf. Ser.* Submitted.
(48) Debenedetti, P. G.; Stillinger, F. H. Supercooled Liquids and the Glass Transition. *Nature* **2001**, *410*, 259−267.